Received: 24 November 2019 | Revised: 7 October 2020 | Accepted: 20 October 2020

IET Power Electronics

DOI: 10.1049/pel2.12068

The Institution of Engineering and Technology WILEY

ORIGINAL RESEARCH PAPER

Sliding mode controller for extraction and supply of photovoltaic power using switched series parallel sources reduced switch count multilevel inverter

G. Eshwar Gowd[1] | **Dharmavarapu Sreenivasarao**[1] | **Hari Priya Vemuganti**[2]

[1] Electrical Engineering Department, National Institute of Technology Warangal, Telangana, India

[2] Electrical Engineering Department, SR University, Telangana, India

Correspondence
Dharmavarapu Sreenivasarao, Electrical Engineering Department, National Institute of Technology Warangal, Telangana, 506004, India.
Email: luckysrinu@gmail.com

Abstract

The reduced switch count multilevel inverter (RSC-MLI) is the latest trend in power electronic converters due to reduction in the switch count and cost. However, a large number of RSC-MLIs have not yet reached to the application level because of the absence of modularity, unequal load-sharing among DC sources and the absence of switching redundancies. On the other hand, multilevel dc-link (MLDCL) and switched series parallel sources (SSPS) RSC-MLI topologies are modular structures with adequate switching redundancies and can be an alternative to conventional cascaded H-bridge (CHB) for grid-connected photovoltaic (PV) systems. Therefore, in this paper, a comprehensive comparison among CHB, MLDCL and SSPS topologies has been carried out for grid connected PV application. Based on the outcome, an asymmetric 11 kV three-phase 11-level SSPS RSC-MLI is chosen. In this combination, a common non-linear sliding mode controller (SMC) is developed for generating maximum PV power from asymmetric single-stage PV sources by linearizing the non-linear PV system using an effective feedback linearization scheme. The PV power extracted is delivered to the grid by controlling SSPS RSC-MLI using another SMC. The performance of the system under wide variations of insolation levels is verified in MATLAB and further validated in hardware-in-the-loop OPAL-RT controller.

1 | INTRODUCTION

Integration of large-scale photovoltaic (PV) power with the grid through two-level inverters is an ineffective process as the switches have limited voltage and current ratings and also require high values of filters. Multilevel inverters (MLIs) are a better choice in order to minimize the disadvantages. This is because they offer low dv/dt, low electromagnetic interference (EMI), low total harmonic distortion (THD) and hence apparently decrease the weight and size of filter components. Amongst all conventional MLIs [1], cascaded H-bridge (CHB) MLI has gained greater prominence in applications such as grid interfacing of PV systems, because, it is modular structure and consists of separate dc sources for each H-bridge module. However, the requirement of a large number of switches at higher levels has led to an increase in system complexity, losses, size and cost. The demerits of CHB discourage its application in high-power applications. In recent times, a large number of reduced switch count (RSC) MLI topologies have been introduced to reduce the number of switching devices for a given number of levels compared to CHB MLI. Hence, it is necessary to choose an alternate topology for CHB MLI by reviewing the recently introduced RSC-MLI for grid tied PV based applications.

An overview of various topological structures of RSC-MLIs is presented in [2, 3]. Among which, T-type RSC based MLI reported in [4] has a significant reduction in power semiconductor devices compared to conventional MLIs. However, this configuration requires bidirectional switches with different voltage ratings and equal load sharing among the dc sources, which is not possible. Another topology, in which 'sources are connected in series through switches' (SCSS), is reported in [5]. This topology is highly modular in structure and the highest rated switches can be operated at fundamental frequency. On the other hand, equal load sharing and asymmetry in sources is

not possible and switches have different voltage ratings which makes load sharing even more difficult. The topology which is introduced in [6] consists of all bidirectional switches so that the number of gate driver circuits can be reduced. However, equal load sharing of sources is not possible and the highest voltage rating switches operate at switching frequency. The topologies presented in [7–9] consist of single input dc source. Further, MLI [7] affords the benefit of peak reverse voltages present across all the switches which is equal to dc input voltage. However, the adoption of asymmetric PV sources to these topologies of [7–9] is not possible. The topology presented in [10] and 'reversing voltage' (RV) modular MLI topology [11] have the feature of common dc input for three-phase realization, thereby allowing saving in terms of input dc sources. Nevertheless, the asymmetric nature in voltage sources and equal load sharing is not possible with this topology [11]. Another topology presented in [12] requires fewer switch count, fewer dc sources and it reduces the number of ON state switches with reduction in the number of gate driver involvement. The cascaded 'half-bridge based multilevel dc-link' (MLDCL) MLI presented in [13, 14] is simple and highly modular in its structure, which requires unidirectional switches only, and the high rating switches operate at fundamental frequency. Another topology with 'switched series/parallel sources' (SSPS) MLI [15] has related advantages of MLDCL MLI. SSPS and MLDCL MLIs can overcome most of the drawbacks that exist in the above mentioned topologies. Moreover, the requirement of isolated dc sources and low control complexity, makes these, an ideal candidate for grid connected distributed power generation applications. Hence, SSPS and MLDCL RSC-MLIs are viable alternatives to CHB MLI for converting dc to ac in grid tied PV based systems.

The grid interfacing of PV systems through conventional CHB MLI with appreciable control objectives is discussed in [16–22]. In order to achieve the objectives, the conventional PI controllers are adopted in [16–22]. However, MLI based grid connected PV system is highly complex and non-linear. Practically, these non-linear systems degrade the performance of linear PI controllers during parameter changes and operating point shifting. In particular, obtaining of controlled maximum power from PV sources using linear PI control during insolation varying conditions is a critical task [16–22]. Because of fixed gains of PI controller, it can be tuned for generating maximum power at a specific range of irradiance level only. For other irradiance levels, the designed gains of PI controller may not be suitable to extract accurate maximum power from PV sources. Further, the highly non-linear grid tied PV system may become unstable during irradiance and environmental changes, because of unsuitability of the fixed gain PI controller. Further, the tuning of gains become difficult in case of independent PV power control of each sources connected to input of each module of the CHB MLI. Therefore, a large number of PI controllers are needed to obtain the maximum power from all PV sources.

CHB-MLI based grid tied PV systems proposed in [18, 19] are dual stage systems which include DC–DC converters. These dual-stage systems are highly non-linear, complex, generate heavy losses, and are expensive compared to single stage systems. Hence, the process of extraction of maximum power from PV source of each dual-stage H-bridge module of CHB MLI, and the process supply of PV power into the grid through controlled MLI has become cumbersome process by using a large number of PI controllers. Moreover, the demerits of CHB MLI discourage its use in high-power applications. To minimise these problems, the existing CHB MLI based grid interfaced PV system under linear PI controller is needed to be replaced with a suitable RSC MLI based grid connected PV system under the control of a robust non-linear controller.

Hence, for obtaining accurate desired power from PV sources and feeding it into grid, it is compulsory to linearize both non-linear photovoltaic system and non-linear MLI based grid connected system. For this, an effective linearization scheme and a robust control mechanism is needed which must be insensitive to irradiance changes, system operating point changes and uncertainties. One of such linearization method is feed-back linearization and non-linear robust control scheme is sliding mode control (SMC). The control of two-level inverter based grid system using SMC under various operating points and system parameter changes is reported in [23, 24]. Nevertheless, extraction of maximum power in single-stage MLI based grid tied PV system using SMC is not yet presented. Control of PV power using other various controllers such as neural network control and fuzzy logic control are developed for dual-stage and single-stage two-level inverter based grid systems in [25–28]. However, the implementation of SMC for PV power extraction is easier than fuzzy and neural network controllers.

Therefore, the main objective of this paper is adoption of SMCs for both extraction and supplying of photovoltaic power to the grid through suitable RSC MLI. In order to choose superior RSC MLI, a comprehensive comparative analysis has been carried out among eleven-level asymmetric CHB MLI, MLDCL and SSPS RSC MLIs by considering various factors such as device count, blocking voltages, operating frequency of switches, rating of switching devices and utilization of input sources. Based on this, an asymmetrical 11 kV three-phase eleven-level SSPS MLI is chosen for grid integration of single-stage PV system. To demonstrate even power sharing among PV sources, asymmetrical sources with 1:2:2 ratio is considered. For achieving maximum power from PV sources, an effective feed-back linearized scheme and a robust SMC is established. In this process, a common SMC based maximum power point track (MPPT) controller is implemented for obtaining maximum PV power from each group of the same rated PV sources of three-phase SSPS topology. Further, the PV power extracted is supplied to the grid through controlled SSPS MLI using another SMC. The superior performance of the established SMC is confirmed against the conventional PI for providing the desired PV powers under various irradiance levels and disturbances using MATLAB and in HIL real-time platforms. Further, the even power sharing among PV sources of SSPS MLI and accurate desired power obtained from all PV generators using designed SMC scheme is verified for wide variations of irradiance levels in simulation environment and further the results are confirmed in real-time environment using OPAL-RT [29] modules.

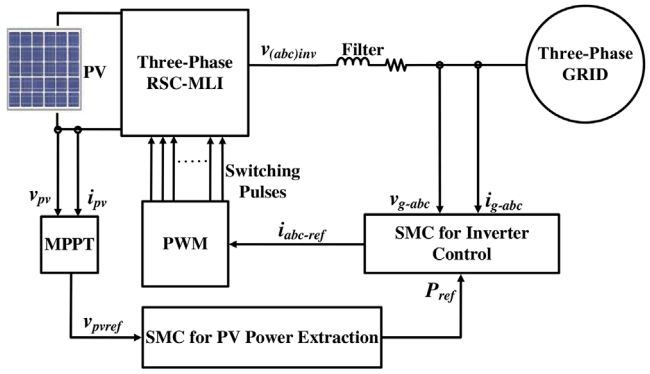

FIGURE 1 Grid connected PV based MLI system layout

The rest of the paper is organized as follows. Section 2 describes an outline of the proposed closed-loop system. The topological structure and comparative analysis between CHB, MLDCL and SSPS RSC-MLIs is discussed in Section 3. Modular improvements of SSPS MLI are discussed in Section 4. Linearization of both PV system and MLI based grid connected system is described in Section 5. Application of SMC for generating and supplying of maximum power from PV source into the grid through SSPS MLI is analyzed in Section 6. Simulation studies and their validation in real-time environment are reported in Section 7.

2 | OVERVIEW OF THE PROPOSED SYSTEM MODEL

The schematic view of a closed-loop control system which includes grid connected RSC-MLI with PV source as input is shown in Figure 1. For obtaining the maximum power of PV sources, the V_{pvref} generated from MPPT algorithm is given to SMC. The output of SMC is controlled maximum power (P_{ref}) of PV sources for a given irradiance level. The supply of PV power (P_{ref}) into the grid is supported by controlling RSC-MLI using another SMC, which generates the reference modulating signals for implementing PWM scheme of MLI, as presented in Figure 1.

3 | RSC-MLI TOPOLOGIES

Among existing RSC-MLI configurations in the literature, MLDCL [13] and SSPS [15] MLIs are dominant topologies for grid integration of PV based applications. These topologies not only require reduced number of switch count but also they are highly modular in their structure and offer the following structural benefits.

1. There is a possibility to connect asymmetrical PV sources to further reduce switch count.
2. The structures of MLDCL MLI and SSPS MLI allow even power issue between equal rating PV sources [2]. Therefore, a single maximum PV power generating control strategy can be applied for multiple same rating PV sources, thereby reducing the control complications.
3. Due to series/parallel connection of dc voltage sources in SSPS MLI, all input dc sources are utilised in most of the voltage levels. Therefore,
4. Utilisation factor (UF) of input dc sources of this topology is more compared to UF in conventional CHB MLI and other RSC MLIs.
5. Further, the highest rating switches in polarity generator of MLDCL and SSPS MLI as shown in Figure 2(b,c) are operating at fundamental frequency. This will reduce switching losses. Whereas in CHB MLI, shown Figure 2(a), all the switches operate at switching frequency.

Owing to these reasons, MLDCL and SSPS RSC-MLIs have the potential to be viable alternative to CHB MLI. To further identify a superior topology for adopting PV application, a comprehensive comparison is presented among CHB, MLDCL and SSPS topologies. For this comparison, 11-level inverters are considered with PV source voltage in the ratio of 1: 2: 2, shown in Figure 2.

3.1 | Single-phase 11-level asymmetric SSPS MLI and asymmetric MLDCL MLI

The structure of eleven-level asymmetric CHB MLI is shown in Figure 2(a). The structure of eleven-level asymmetric MLDCL topology [13] is shown in Figure 2(b), and is divided into level generator and polarity generator. The first one is responsible for producing uni-polar voltage while the latter has H-bridge in each phase with switches operating at fundamental frequency and this converts uni-polar voltage into bipolar. In Figure 2(b), level generation structure can be configured by cascading three half-bridge modules and each bridge module consists of a PV source.

Figure 2(c) shows the single-phase asymmetric eleven-level SSPS MLI which consists of upper and lower parts. The lower part consist of a modular structure with sources $\text{PV}_{1a} = \text{PV}_{2a} = 2V_{\text{dc}}$. In order to obtain more voltage levels, a H-bridge (upper part) with source $\text{PV}_{0a} = V_{\text{dc}}$ is in cascade connection with lower/modular part. The specific feature of SSPS MLI is that different levels in the output voltage can be attained by series/parallel connection of PV sources. This will enable the topology to contribute power to the grid from all PV sources at all voltage levels. Therefore, the utilization of sources of SSPS MLI is more related to other MLI topologies in which all the sources are connected only at peak level of output voltage.

3.2 | Comparative analysis among 11-level asymmetric CHB, MLDCL and SSPS MLIs

The comparative study among the conventional CHB MLI and RSC-MLIs is done by critically comparing different factors which would be helpful in finding superior topology for PV application.

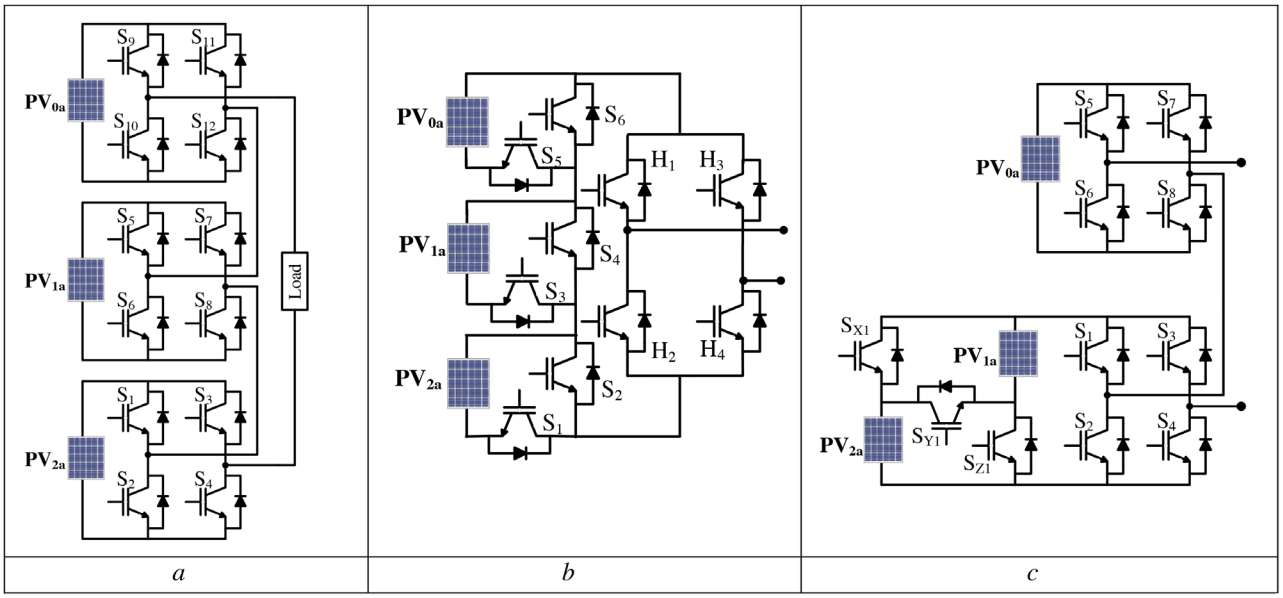

FIGURE 2 Eleven-level asymmetric ($PV_{1a} = PV_{2a} = 2V_{dc}$ and $PV_{0a} = V_{dc}$) CHB and RSC-MLI topologies. (a) CHB MLI (b) MLDCL MLI (c) SSPS MLI

3.2.1 | Switch count

In asymmetric CHB MLI shown in Figure 2(a), the number of switches required for phase to generate 11-levels in output phase-voltage is 12, whereas in asymmetric SSPS MLI and MLDCL MLI, the switch count is 11 and 10 respectively. Hence in order to obtain voltage levels in the output voltage, more number of switches should conduct in CHB compared to SSPS and MLDCL MLI. For example, the number of switches in conduction for obtaining $3V_{dc}$ voltage level of eleven-level output voltage of CHB, MLDCL and SSPS MLIs shown in Figure 2 are 6, 5, and 5 respectively. Hence, conduction losses in CHB MLI are more compared to SSPS and MLDCL MLIs. The losses are highly considerable if the number of voltage levels increases in the output voltage.

3.2.2 | Utilization factor of DC sources in MLIS

In order to estimate the active use of dc sources in MLI, a parameter UF is introduced. If 'X_i' is the number of dc sources connected to MLI for obtaining specific level (i) in output voltage of MLI: 'N' is the number of phase voltage levels and 'M' is the number of dc sources, the UF is determined as:

$$\mathrm{UF} = \frac{\text{Sum of the number of voltage source connected to MLI at each phase voltage level}}{\left(\begin{array}{c}\text{Total number of phase voltage level}\\ \times \\ \text{total number of source of the MLI}\end{array}\right)} \quad (1)$$

$$\mathrm{UF} = \frac{\sum_{i=1}^{n} X_i}{N \times M}$$

TABLE 1 PV sources connected to MLI at each voltage level for 11-level asymmetric SSPS and MLDCL (or) CHB MLIs with $PV_{1a} = PV_{2a} = 2V_{dc}$ and $PV_{0a} = V_{dc}$

Phase voltage level	No. of Connected dc sources in SSPS	No. of Connected dc sources in CHB (or) MLDCL
$+5V_{dc}$	PV_{1a}, PV_{2a}, PV_{0a} (3)	PV_{1a}, PV_{2a}, PV_{0a} (3)
$+4V_{dc}$	PV_{1a}, PV_{2a} (2)	PV_{1a}, PV_{2a} (2)
$+3V_{dc}$	PV_{1a}, PV_{2a},V_{0a} (3)	PV_{1a}, PV_{2a}, PV_{0a} (3)
$+2V_{dc}$	PV_{1a}, PV_{2a} (2)	PV_{2a} (1)
$+V_{dc}$	PV_{1a}, PV_{2a}, PV_{0a} (3)	PV_{1a}, PV_{0a} (2)
0	0	0
$-V_{dc}$	PV_{1a}, PV_{2a}, PV_{0a} (3)	PV_{1a}, PV_{0a} (2)
$-2V_{dc}$	PV_{1a}, PV_{2a} (2)	PV_{1a} (1)
$-3V_{dc}$	PV_{1a}, PV_{2a}, PV_{0a} (3)	PV_{1a}, PV_{2a}, PV_{0a} (3)
$-4V_{dc}$	PV_{1a}, PV_{2a} (2)	PV_{1a}, PV_{2a} (2)
$-5V_{dc}$	PV_{1a}, PV_{2a}, PV_{0a} (3)	PV_{1a}, PV_{2a}, PV_{0a} (3)

Table 1 shows the number of dc sources connected for generating a specific level in output phase voltage of the considered MLIs. The UFs of DC sources of 11-level considered MLIs can be calculated using Equation (1) and Table 1. From Table 1, it is observed that the number of dc sources connected to CHB and MLDCL are the same at every voltage level. Hence, UFs of CHB and MLDCL MLI are equal. The UFs of DC sources of 11-level and 19-level asymmetric CHB MLI, MLDCL MLI, and SSPS MLI are presented in Table 2.

From Table 2, it is observed that the UF of SSPS MLI is significantly higher compared to the same level CHB and MLDCL. Higher utilization of input sources allows the inverter to generate more power in applications such as PV.

TABLE 2 Utilization factor (UF) of 11- and 19-level asymmetric MLDCL (or) CHB and SSPS RSC-MLI topologies

Phase-voltage levels	UF of SSPS	UF of MLDCL (or) CHB MLI
11	0.866	0.6
19	0.911	0.644

TABLE 3 Operating frequencies of various switches of asymmetric MLDCL and SSPS MLI

SSPS MLI		MLDCL MLI	
Switches	Operating frequency	Switches	Operating frequency
S_{x1}, S_{y1}, S_{z1}	$2f_m$	None	
S_5, S_6, S_7, S_8	f_c	$S_1, S_2, S_3, S_4, S_5, S_6$	f_c
S_1, S_2, S_3, S_4	f_m	H_1, H_2, H_3, H_4	f_m

3.2.3 | Current rating of DC sources and switches

In order to record the currents delivered by each dc source in the considered inverters, a simulation study is performed. In this study, the dc voltages selected are 1600, 3200, and 3200 V. Figures 3(a) and 3(b) show the current waveforms of each DC sources in eleven-level asymmetric MLDCL MLI and SSPS MLI respectively for a resistive load of 0.8 MW/Ph. Since utilization of dc sources of both CHB and MLDCL MLIs is equal, the peak currents delivered from their dc sources are same. Hence, the waveform of currents passing through dc sources of MLDCL MLI shown in Figure 3(a) are valid for currents of dc sources in CHB MLI.

From Figure 3 it can be observed that the peak value of the current waveforms of the DC sources in CHB and MLDCL is nearly double that of the peak value of current waveforms of DC sources in SSPS inverter. Therefore, for a given number of voltage levels, phase-voltage value and power rating, the switches and dc sources in SSPS inverter require lower current ratings compared to CHB and MLDCL.

3.2.4 | Operating frequency of the switches

Table 3 shows the operating frequency of each switch in SSPS and MLDCL MLIs of Figure 2. Here, f_c and f_m are carrier and modulating signal frequencies respectively. From Table 3, it is clear that more switches in 11-level asymmetric MLDCL MLI are operating at carrier frequency compared to SSPS. Therefore, switching losses in asymmetric MLDCL are more compared to that in SSPS. In case of CHB MLI shown in Figure 2(a), all the switches operate at carrier frequency. Hence, switching losses of CHB MLI are higher compared to MLDCL and SSPS MLI.

3.2.5 | Total blocking voltage of an inverter

For asymmetric PV sources (V_{dc}: $2V_{dc}$: $2V_{dc}$) shown in Figure 2, the 'total blocking voltage [2]' of CHB MLI, SSPS MLI and MLDCL MLI are $20V_{dc}$, $26V_{dc}$ and $30V_{dc}$ respectively. Therefore, an 11-level asymmetric SSPS MLI has lower blocking voltage compared to MLDCL MLI, which in turn reduces the cost.

From the above five factors, it is concluded that asymmetric SSPS RSC MLI is optimised superior to both CHB MLI and MLDCL RSC MLI, especially in device switching frequency, utilization of dc sources and current rating of switches. In view of this, SSPS MLI is considered for grid interfaced PV system and discussed hereafter.

4 | MODULAR IMPROVEMENTS OF SSPS RSC MLI FOR EASY IMPLEMENTATION OF PV POWER EXTRACTION CONTROL STRATEGY

The modular improvements of the SSPS RSC MLI is possible by increasing the number of equal rated sources in the modular structure of the SSPS MLI as shown in Figure 4. The number of sources in this modular structure is either odd or even in

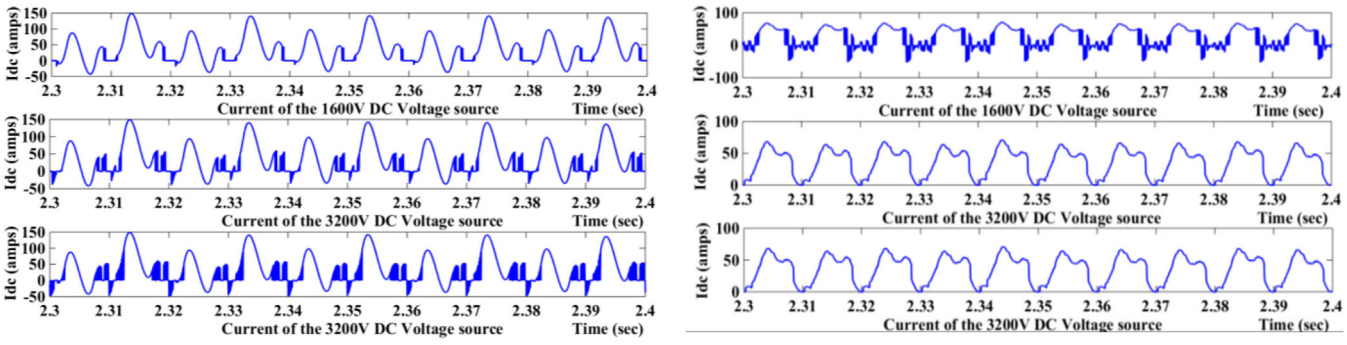

FIGURE 3 The currents passing through each dc source of MLDCL and SSPS MLIs. (a) Currents passing through DC voltage source of MLDCL MLI. (b) Currents passing through DC voltage source of SSPS MLI

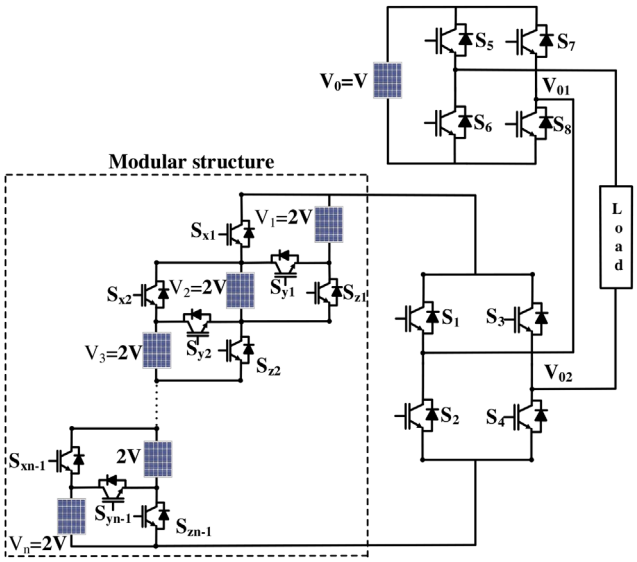

FIGURE 4 Generalised structure of asymmetric SSPS MLI

number. The feasibility of power extraction control method for odd and even number of PV sources is discussed below.

4.1 | Odd number of equal rated PV sources is connected

In the modular part of the asymmetric (i.e. input dc voltage ratio of 1:2:2) SSPS MLI of Figure 4, if odd number of 2 V rated PV sources will connect then there exist lack of redundancies for generating the output voltage levels. Because of the lack of redundancies, the average current passing through all 2 V rated PV sources is not equal therefore, it is not possible to implement a common MPPT control for all 2 V rated PV sources. Thus, it necessitates individual MPPT controllers which leads to increased control complexity. The modular structure of SSPS MLI with three PV sources is shown in Figure 5(a). The generation of voltage levels from this modular structure and average current passing through PV_1, PV_2 and PV_3 sources of Figure 5(a) at every voltage levels are given in Table 4. From Figure 5(a) and Table 4 it is observed that even though PV_1, PV_2 and PV_3 have equal voltage rating of 2 V, however for generating 4 V voltage level, the average current passing through PV_2 source is lower compared to the average current through PV_1 or PV_3. Hence, there is a separate power extraction control method is required for PV_2 source.

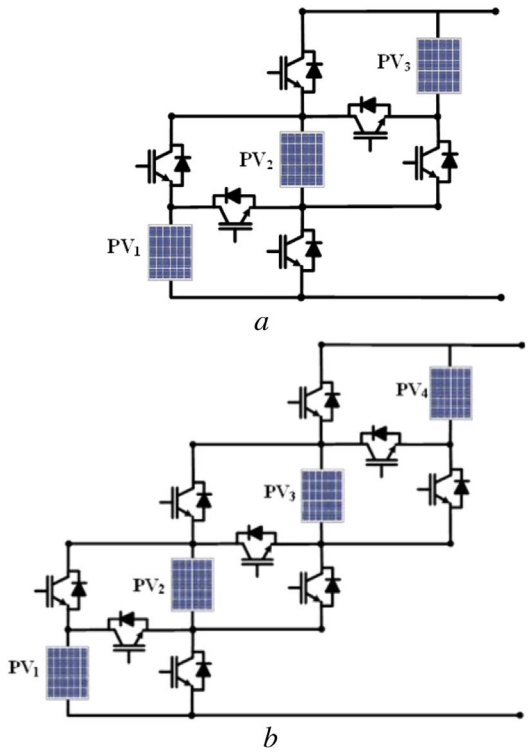

FIGURE 5 Modular improvements of asymmetric SSPS MLI. (a) Odd number of sources connected to modular structure of SSPS MLI. (b) Even number of sources connected to modular structure of SSPS MLI

4.2 | Even number of equal rated PV sources are connected

In the modular part of the asymmetric SSPS MLI of Figure 4, if even number of 2 V rated PV sources will connect then adequate switching redundancies are developed. Because of these redundancies, the average current passing through all 2 V rated PV sources is equal and therefore, a common control strategy can be implemented for all 2 V rated PV sources, thereby reducing control complexity. The modular structure of SSPS MLI with four PV sources is shown in Figure 5(b). The generation of voltage levels from this modular structure and average current passing through PV_1, PV_2, PV_3 and PV_4 sources of Figure 5(b) at every voltage levels is given in Table 5. From Figure 5(b) and Table 5, it is observed that the average current passing through these equal rated PV sources is equal at all voltage levels. Hence, a common control strategy can be applied for desired PV power extraction form PV_1, PV_2, PV_3 and PV_4 sources with ease.

TABLE 4 Generation of voltage levels form odd number of 2 V rated PV sources connected in modular structure of SSPS MLI

Voltage levels	Connection of PV sources for generating output voltage level	Average current passing through all '2 V' rated PV sources
6 V	PV_1, PV_2 and PV_3 are connected in series.	Equal
4 V	The parallel connection of PV_1 and PV_2 is connected in series with PV_3. (or) The parallel connection of PV_2 and PV_3 is connected in series with PV_1.	Unequal (This is due to the average current passing through PV_2 is half of the current through PV_3 or PV_1).
2 V	PV_1, PV_2 and PV_3 are connected in parallel.	Equal

TABLE 5 Generation of voltage levels form even number of 2 V rated PV sources connected in modular structure of SSPS MLI

Voltage levels	Connection of PV sources for generating output voltage level	Average current passing through all '2 V' rated PV Sources
8 V	PV_1, PV_2, PV_3 and PV_4 are connected in series.	Equal
6 V	PV_1, PV_2 and PV_3 are connected in series and PV_4 is connected in parallel with PV_3. (or) PV_2, PV_3 and PV_4 are connected in series and PV_1 is connected in parallel with PV_2.	Equal
4 V	The parallel connection of PV_1 and PV_2 is connected in series with the parallel connection of PV_3 and PV_4.	Equal
2 V	PV_1, PV_2, PV_3 and PV_4 are connected in parallel	Equal

Note: In Tables 4 and 5, the remaining levels in the output voltage can be obtained by summing the output voltage of upper H-bridge connected in cascade with modular part of SSPS MLI.

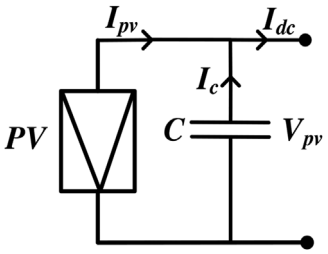

FIGURE 6 Photovoltaic source

5 | LINEARIZATION OF PROPOSED PV BASED GRID CONNECTED SSPS MLI SYSTEM

This section discusses the input-output linearization method to develop non-linear controllers for obtaining maximum power of PV source and for controlling the grid tied SSPS MLI. Once the linearized mathematical models are developed for non-linear PV system and for grid connected MLI, a robust SMC scheme can be designed for obtaining non-linear control quantities.

5.1 | Linearization of non-linear PV generator

The non-linear conversion of PV systems includes the execution of feedback-linearization control scheme. This technique can prevent the degraded behaviour of controller due to non-linearities of the PV system. Additionally, this technique has the ability to endure the PV system to be controlled for a wide-ranging of irradiance conditions.

The PV source, shown in Figure 6 with a parallel capacitor C can be defined in terms of mathematical dynamic Equations (2) and (3):

$$I_{\mathrm{pv}} + I_{\mathrm{c}} = I_{\mathrm{dc}} \tag{2}$$

$$I_{\mathrm{pv}} + C\frac{\mathrm{d}V_{\mathrm{pv}}}{\mathrm{d}t} = I_{\mathrm{dc}} \text{ or } \frac{\mathrm{d}V_{\mathrm{pv}}}{\mathrm{d}t} = -\frac{1}{C}I_{\mathrm{pv}} + \frac{1}{C}I_{\mathrm{dc}} \tag{3}$$

where I_{dc}, I_{pv} and I_{c} are dc-link current, PV current and capacitor current respectively.

In order to linearize the PV system, non-linear Equation (3) has to be linearized by modifying it into standard state space equation as shown below:

$$\frac{\mathrm{d}x_{\mathrm{pv}}}{\mathrm{d}t} = f_{\mathrm{pv}}(x) + g_{\mathrm{pv}}(x)u_{\mathrm{pv}} \tag{4}$$

The state space representation of the PV source can be realized by rearranging Equation (3) in the form of Equation (4) with V_{pv} as state-variable which results in Equation (5).

$$\begin{aligned} x_{\mathrm{pv}} &= [V_{\mathrm{pv}}]\ u_{\mathrm{pv}} = [I_{\mathrm{dc}}] \\ g_{\mathrm{pv}}(x) &= \left[\frac{1}{C}\right]\ f_{\mathrm{pv}}(x) = \left[\frac{-1}{C}I_{\mathrm{pv}}\right] \end{aligned} \tag{5}$$

After linearization, the new system with linearization can be defined as:

$$U_{pv} = g_{pv}^{-1}(x_{pv})\left(\lambda_{pv} - f_{pv}(x_{pv})\right) \tag{6}$$

Equation (6) can also represent in the following form as:

$$U_{\mathrm{pv}} = \alpha_{\mathrm{pv}}(x_{\mathrm{pv}}) + (\beta_{\mathrm{pv}}(x_{\mathrm{pv}}) \times \lambda_{\mathrm{pv}}) \tag{7}$$

where, $\alpha_{\mathrm{pv}}(x_{\mathrm{pv}}) = -{g_{\mathrm{pv}}}^{-1}(x_{\mathrm{pv}}) \times f_{\mathrm{pv}}(x_{\mathrm{pv}}), \beta_{\mathrm{pv}}(x_{\mathrm{pv}}) = {g_{\mathrm{pv}}}^{-1}(x_{\mathrm{pv}})$ and λ_{pv} is the state vector matrix with $\mathrm{d}V_{\mathrm{pv}}/\mathrm{d}t$ as an element that is,

$$\lambda_{\mathrm{pv}} = [\lambda_{11}]^T = \left[\frac{\mathrm{d}V_{\mathrm{pv}}}{\mathrm{d}t}\right]^T \tag{8}$$

Here, the output voltage of PV source is V_{pv}. Therefore the output matrix can be defined as:

$$Y = [V_{\mathrm{pv}}] \tag{9}$$

5.2 | Linearization of non-linear grid tied MLI system

In order to supply maximum power of all input PV sources of SSPS MLI into the grid, the three-phase SSPS MLI should

be efficiently controlled for wide variations in irradiance conditions. However, grid tied MLI based system is highly nonlinear which affects the performance of the controller. It is necessary to develop a dynamic model of MLI based grid system for converting non-linear system into linear system. The non-linear transformation of the MLI based grid system involves feedback linearization scheme in which output is forced to follow input in a closed-loop manner.

The dynamic equation between SSPS MLI and grid in *d–q* frame of reference [23] is:

$$V_{\mathrm{dinv}} - R_{\mathrm{f}} i_{\mathrm{dg}} - L_{\mathrm{f}} \frac{\mathrm{d}i_{\mathrm{dg}}}{\mathrm{d}t} + wL_{\mathrm{f}} i_{\mathrm{qg}} - V_{\mathrm{dg}} = 0 \tag{10}$$

$$V_{\mathrm{qinv}} - R_{\mathrm{f}} i_{\mathrm{qg}} - L_{\mathrm{f}} \frac{\mathrm{d}i_{\mathrm{qg}}}{\mathrm{d}t} - wL_{\mathrm{f}} i_{\mathrm{dg}} - V_{\mathrm{qg}} = 0 \tag{11}$$

where, V_{dinv}, V_{qinv} are inverter voltages, i_{dg}, i_{qg} and V_{dg}, V_{qg} are grid currents and voltages respectively.

Consider the standard state space equation below:

$$\frac{\mathrm{d}x_{\mathrm{inv}}}{\mathrm{d}t} = f_{\mathrm{inv}}(x) + g_{\mathrm{inv}}(x) u_{\mathrm{inv}} \tag{12}$$

The non-linear and coupled MLI based grid system can be converted to linear and decoupled system by transforming Equations (10) and (11) in the form of state space Equation (12).Thus, the system matrix, input matrix, variable matrix, and control input matrix obtained are given below.

$$\begin{aligned} f_{\mathrm{inv}}(x) &= \begin{bmatrix} -\frac{R_{\mathrm{f}}}{L_{\mathrm{f}}} i_{\mathrm{dg}} + \frac{X_{\mathrm{f}}}{L_{\mathrm{f}}} i_{\mathrm{qg}} - \frac{1}{L_{\mathrm{f}}} V_{\mathrm{dg}} \\ -\frac{R_{\mathrm{f}}}{L_{\mathrm{f}}} i_{\mathrm{qg}} - \frac{X_{\mathrm{f}}}{L_{\mathrm{f}}} i_{\mathrm{dg}} - \frac{1}{L_{\mathrm{f}}} V_{\mathrm{qg}} \end{bmatrix} X = \begin{bmatrix} i_{\mathrm{dg}} \\ i_{\mathrm{qg}} \end{bmatrix} \\ g_{\mathrm{inv}}(x) &= \begin{bmatrix} \frac{1}{L_{\mathrm{f}}} & 0 \\ 0 & \frac{1}{L_{\mathrm{f}}} \end{bmatrix} U_{\mathrm{inv}} = \begin{bmatrix} V_{\mathrm{dinv}} \\ V_{\mathrm{qinv}} \end{bmatrix} \end{aligned} \tag{13}$$

After linearization, the system can be represented for obtaining inverter control input U_{inv} as:

$$U_{\mathrm{inv}} = (-{g_{\mathrm{inv}}}^{-1}(x) \times f_{\mathrm{inv}}(x)) + ({g_{\mathrm{inv}}}^{-1}(x) \times \lambda_{\mathrm{inv}})$$

(or)

$$U_{\mathrm{inv}} = \alpha_{\mathrm{inv}}(x) + \beta_{\mathrm{inv}}(x) \lambda_{\mathrm{inv}} \tag{14}$$

where, λ_{inv} is state vector matrix and is represented as:

$$\lambda_{\mathrm{inv}} = [\lambda_{11}\ \lambda_{12}]^T = \left[\frac{\mathrm{d}i_{\mathrm{dg}}}{\mathrm{d}t}\ \frac{\mathrm{d}i_{\mathrm{qg}}}{\mathrm{d}t} \right]^T \tag{15}$$

In the proposed grid tied MLI system, the output states are considered as:

$$Y_{\mathrm{inv}} = [i_{\mathrm{dg}}\ i_{\mathrm{qg}}]^T \tag{16}$$

6 | APPLICATION OF SLIDING MODE CONTROL AND FORMULATION

Sliding mode control [23, 24] is a robust control scheme and it can be tested for the control of non-linear and linear systems. Because of its infinite gain, it overrides the errors accomplice with system uncertainties, parameter changes and operating point shifting in the system. In this control scheme, the state of the system is turned out toward the sliding surface and alternated up to equilibrium point. The sliding surface and switching do not depend on the converter dynamics, operating point and circuit parameters. In this paper, SMC scheme is adopted to derive new λ_{pv}, λ_{inv} and consequently U_{pv} and U_{inv} in Equations (7) and (14) respectively for achieving controlled PV power and for control of grid tied MLI respectively.

6.1 | Design of SMC for maximum power control of PV system

6.1.1 | Formation of sliding surface and concept of stability

The state vector matrix, λ_{pv} obtained in linearization procedure of PV system is the input of SMC and it is going to adjust from old to new state vector as far as the actual value of variable quantity reaches reference value. The output from SMC is reference control $U_{\mathrm{pv}}(t)$, that is, I_{dcref} which is important for generating maximum power from PV source. $U_{\mathrm{pv}}(t)$ is a combination of switching control and equivalent control as shown in Equation (17). Equivalent control can be attained from the procedure of system linearization whereas switching function is responsible for the procedure of nullifying the errors in output states.

$$U_{\mathrm{pv}}(t) = U_{\mathrm{eq}}(t) + U_{\mathrm{sw}} = U_{\mathrm{eq}}(t) + k.\mathrm{sign}(\sigma_{\mathrm{pv}}) \tag{17}$$

where k is a positive constant value and σ_{pv} is the sliding surface. In order to achieve appropriate operation of the controller, it is needed to control sliding surface. There is only one sliding surface (σ_1), because Equation (9) has only one output state. The error in the output (V_{pv}) is chosen as sliding surface and is defined in Equation (18) as a function of error.

$$\sigma_{\mathrm{pv}} = \mathrm{error} = (V_{\mathrm{pv}} - V_{\mathrm{pvref}}) \tag{18}$$

The state of the PV source is directed by SMC near to the equilibrium condition and it is attained by analysing Lyapunov approach given below:

$$L_{\mathrm{pv}} = \frac{1}{2} {\sigma_{\mathrm{pv}}}^2 \tag{19}$$

According to Lyapunov stability theorem, PV system is asymptotically stable if L_{pv} is positive definite and its

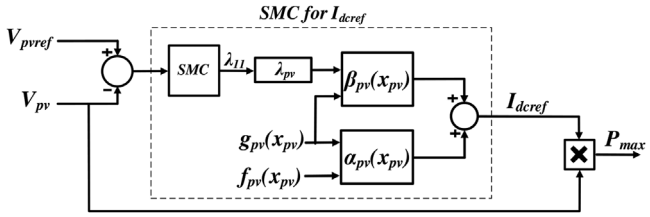

FIGURE 7 Realisation of maximum power from PV source using SMC

differentiation that is, dL_{pv}/dt is a negative definite.

$$\text{i.e. } \frac{dL_{pv}}{dt} = (\sigma_{pv} \times \dot{\sigma}_{pv}^{T}) < 0 \tag{20}$$

To correlate the above condition,$(\sigma_{pv} \times \dot{\sigma}_{pv}^{T}) < 0$, $\dot{\sigma}_{pv}$ can be represented as k.sign(σ_{pv}).

$$\text{i.e. } \dot{\sigma}_{pv} = -k.\text{sign}(\sigma_{pv}) \tag{21}$$

In spite of that, the controller adaptation is highly chattering due to the 'sign' function and it is a hard shifting function. In order to strengthen the controller execution without chattering and for continuous switching, a hyperbolic tangent: tan h' function [23] is chosen in this paper.

Hence, according to the newly considered 'tan h' soft switching function, Equation (21) is transforms to:

$$\dot{\sigma}_{pv} = -k.\tan h(\sigma_{pv}) \tag{22}$$

Substituting Equation (18) in Equation (22),

$$\dot{\sigma}_{pv} = -k.\tan h(V_{pv} - V_{pvref}) \tag{23}$$

With the attained new dynamics using SMC, the state vector of PV system can be reframed as:

$$\lambda_{pv-new} = [\lambda_{11}] = [-k.\tan h(V_{pv} - V_{pvref})] \tag{24}$$

Where V_{pvref} can be attained from P and O MPPT [24] control algorithm. Realization of I_{dcref} and subsequently the required maximum power from PV source using developed SMC is shown in Figure 7. This control technique is implemented for generation of maximum power from all input PV sources of the three-phase SSPS MLI.

6.2 | Design of SMC for control of grid connected SSPS MLI

6.2.1 | Characterization of sliding surface and stability

Feedback linearization of grid tied MLI system provides state vectors λ_{11} and λ_{12} as given in Equation (15). In this section SMC is applied to attained new λ_{11} and λ_{12} and consequently new control inputs V_{dinv} and V_{qinv} for control of SSPS MLI. Hence, the output of SMC is new control input $U_{inv}(t)$ which is a union of switching control and equivalent control. Equivalent control can be attained from the procedure of system linearization as discussed in section 5.2 while switching control is responsible to keep the state trajectories on the sliding surface and nullify the error in output states. $U_{inv}(t)$ can be represented as similar to Equation (17):

$$U_{inv}(t) = U_{eq}(t) + U_{sw} = U_{eq}(t) + \rho.\text{sign}(\sigma_{inv}) \tag{25}$$

In order to force instantaneous states to sliding modes by the control input, it is essential to determine proper sliding surface (σ_{inv}). Here, two sliding surfaces, namely σ_{1inv} and σ_{2inv} can be defined in this system, since Equation (16) has two output states. The errors in the output states, i_{dg} and i_{qg} are chosen as sliding surfaces σ_{1inv} and σ_{2inv} respectively.

$$\text{Therefore, } \sigma_{inv} = \begin{bmatrix} \sigma_{1inv} & \sigma_{2inv} \end{bmatrix} \tag{26}$$

where $\sigma_{1inv} = er_1 = i_{dg} - i_{dref}$ and

$$\sigma_{2inv} = er_2 = i_{qg} - i_{qref} \tag{27}$$

In order to drive the system towards the equilibrium point, the necessary conditions can be obtained by considering Lyapunov approach as:

$$L_{inv} = \frac{1}{2}{\sigma_{inv}}^2 \tag{28}$$

According to Lyapunov stability theorem, in order to maintain the system to asymptotically stable, L_{inv} should be positive definite and its derivative (dL_{inv}/dt) is a negative definite. that is, $\frac{dL_{inv}}{dt} = (\sigma_{inv} \times \dot{\sigma}_{inv}^{T}) < 0$

In order to satisfy the above condition,$(\sigma_{inv} \times \dot{\sigma}_{inv}^{T}) < 0$, $\dot{\sigma}_{inv}$ can be represented as ρ.sign(σ_{inv}).

$$\text{i.e. } \dot{\sigma}_{inv} = -\rho.\text{sign}(\sigma_{inv}) \tag{29}$$

Since 'sign' function is a hard switching one which affects the controller performance, so that 'tan h' function (soft switching function) is used to improve the performance of the controller without chattering.

Hence Equation (29) is modified as:

$$\dot{\sigma}_{inv} = -\rho.\tan h(\sigma_{inv}) \tag{30}$$

i.e.$\dot{\sigma}_{1inv} = -\rho_1.\tan h(\sigma_{1inv})$ and $\dot{\sigma}_{2inv} = -\rho_2.\tan h(\sigma_{2inv})$

Substituting Equation (27) in Equation (30),

$$\begin{aligned} \dot{\sigma}_{1inv} &= -\rho_1.\tan h(i_{dg} - i_{dref}) \\ \dot{\sigma}_{2inv} &= -\rho_2.\tanh(i_{qg} - i_{qref}) \end{aligned} \tag{31}$$

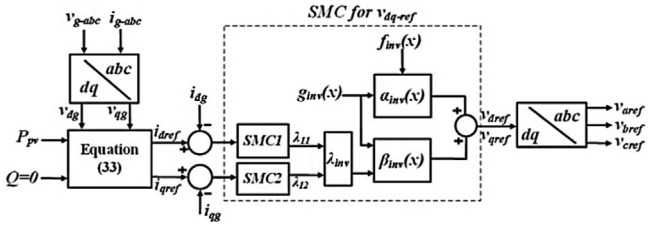

FIGURE 8 Generation of inverter reference voltages using SMC

The new dynamic state vector matrix can be framed as:

$$\lambda_{\text{inv}-\text{new}} = \begin{bmatrix} \lambda_{11\text{new}} \\ \lambda_{12\text{new}} \end{bmatrix} = \begin{bmatrix} -\rho_1 . \tan h(i_{\text{dg}} - i_{\text{dref}}) \\ -\rho_2 . \tan h(i_{\text{qg}} - i_{\text{qref}}) \end{bmatrix} \tag{32}$$

where ρ_1 and ρ_2 are constants. The references i_{dref} and i_{qref} can be obtained from the following standard equations:

$$i_{\text{dref}} = \frac{v_{\text{qg}} Q_{\text{ref}} + v_{\text{dg}} P_{\text{ref}}}{v_{\text{dg}}^2 + v_{\text{qg}}^2} \quad \text{and} \quad i_{\text{qref}} = \frac{v_{\text{qg}} P_{\text{ref}} - v_{dg} Q_{\text{ref}}}{v_{\text{dg}}^2 + v_{\text{qg}}^2} \tag{33}$$

where P_{ref} is the sum of maximum powers of all input PV sources of three-phase SSPS MLI. In this paper, Q_{ref} is considered as zero. The schematic representation of the above procedure for generation of control input U_{inv} and subsequently modulating signals for closed-loop operation of SSPS MLI is shown in Figure 8.

Figure 9 shows the schematic view of implementation of SMCs for both generation of desired power from input PV sources of three-phase SSPS MLI and feeding maximum power to the 11 kV grid by controlling MLI. As the considered three-phase asymmetric configuration shown in Figure 9 consists of PV sources PV_1 and PV_2 with equal I–V characteristics and $I_{\text{pv1}} = I_{\text{pv2}}$, a common SMC based MPPT control strategy can be employed for both PV_1 and PV_2 sources as shown in Figure 9. Hence the control complexity is reduced. The other PV source (i.e. PV_0) is regulated by another SMC based MPPT scheme, because it has half of the I–V ratings of PV_1 and PV_2. In three-phase SSPS MLI, there are three PV_0 sources in upper part and six sources (i.e. three PV_1 and three PV_2) in lower (modular) part. Therefore, for extracting the maximum power from all six PV sources of the modular part of three-phase SSPS MLI, the power of single PV_1 source is multiplied by six. Similarly, the power of single PV_0 source is multiplied by three. The total PV power is the sum of the powers of six PV_1 (or PV_2) sources and three PV_0 sources and it is considered as P_{ref} to the second SMC strategy which will control SSPS MLI to inject power, P_{ref} into the grid as shown in Figure 9.

7 | ANALYSIS OF RESULTS

In this section, the necessity of SMC is discussed by comparing its superior performance with the degraded performance of conventional PI control for PV power extraction under irradiance varying conditions. The robustness of SMC under grid frequency variations is discussed. Further, the power generation capabilities of asymmetric PV sources of three-phase 11-level SSPS MLI under the control of established SMC scheme is verified at various irradiance conditions. The analysis of results with regard to superior performance of SMC, generation and supplying of maximum PV power to the grid has been discussed in both MATLAB/Simulink and OPAL-RT based real-time environments.

7.1 | MATLAB/Simulink based results

The validation of established SMC for PV power generation is discussed by considering PV sources PV_1, PV_2 and PV_0 of SSPS MLI with MPPT voltages of 3200, 3200, and 1600 V at

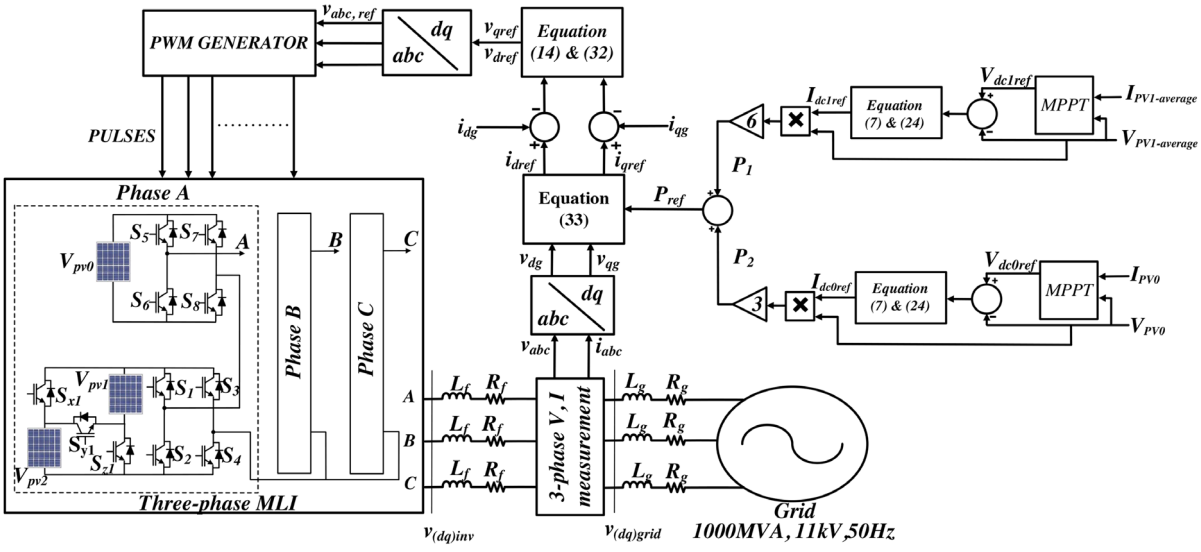

FIGURE 9 Adoption of SMC for injection and extraction of PV power into three-phase 11 kV grid through SSPS MLI

TABLE 6 System parameters

Parameter	Value
Grid voltage, V_g	11 kV
Grid frequency, f	50 Hz
Capacitor across PV panel, C	0.01 F
Filter inductance, L_f	50 mH
Filter resistance, R_f	0.2 Ω
Switching frequency, f_s	5 kHz
Sampling time, T_s	50 μs
Base power	1 MVA
Short-circuit MVA	1000 MVA
Sliding mode parameters k, ρ_1 and ρ_2	11, 3, and 3

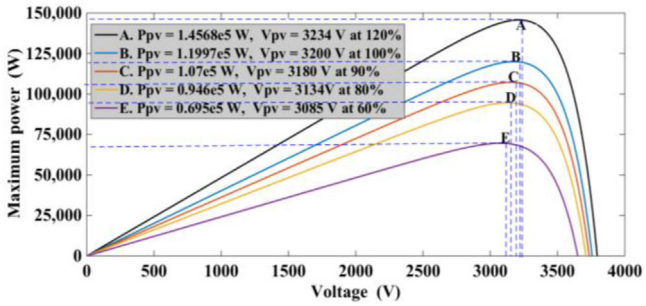

FIGURE 10 P–V characteristics curves of the PV source

an irradiance of 1000 W/m^2 respectively. The parameters used in the simulation study are given in Table 6.

The PV characteristics curve of PV_1 or PV_2 is shown in Figure 10. Points A, B, C, D, and E on the PV characteristics curves in Figure 10 represent the maximum powers and corresponding voltages of PV_1 or PV_2 source at irradiance of 1200, 1000, 900, 800, and 600 W/m^2 respectively. In this paper, 1000 W/m^2 is considered as 100% of irradiance. Figures 11 and 12 represent the phase voltage of 11-level SSPS MLI and its THD spectrum respectively. In Figure 12, the applied switching frequency for hybrid PWM method is $f_s = 5$ kHz. In this PWM method, the authors were implemented with two phase-shifted carrier waveforms (unipolar PWM method). Hence, the dominant harmonics exist around the harmonic order of $2m_f$, that is, 200.

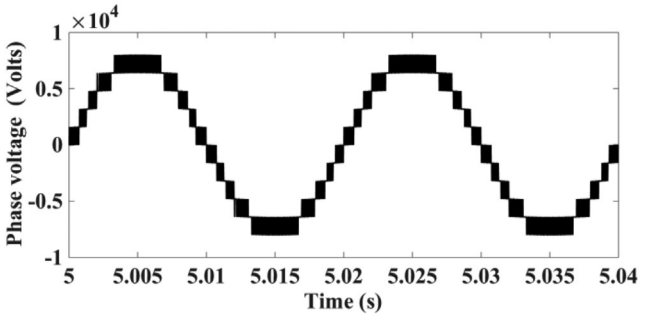

FIGURE 11 Phase voltage waveform of the 11-level SSPS MLI

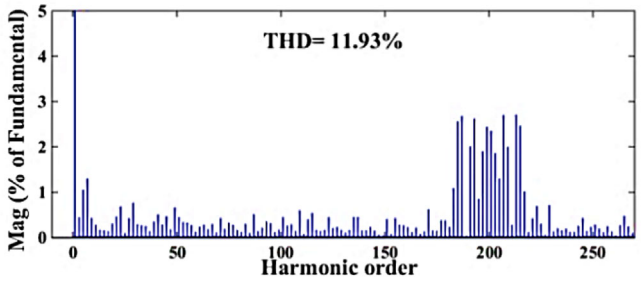

FIGURE 12 THD of eleven level output phase-voltage

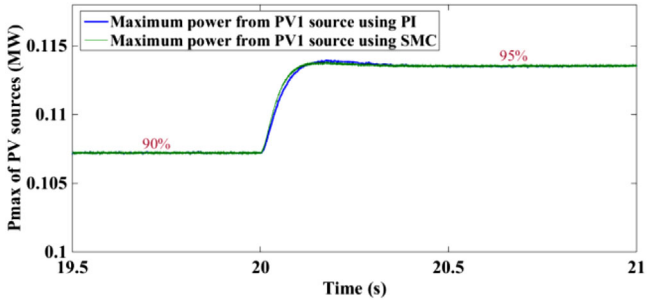

FIGURE 13 Maximum power delivery performance of PI and SMC during insolation varying from 90% to 95%

7.1.1 | Superior performance of SMC over PI controller under irradiance varying conditions

The PI controller is tuned to obtain the desired maximum PV power at a specific irradiance conditions. However, under wide variations in irradiance levels, the same prior tuned parameters of PI controller may not produce a satisfactory response. On the other hand, the parameter of the SMC controller is self -adjusted to produce improved performance under wide variations in irradiance levels. This can be understood by observing Figures 13 and 14, which represent the maximum power responses of PV_1 source of SSPS MLI using PI and SMC controllers. From Figure 13, it can be observed that whenever the irradiance slightly changes from 90% to 95% (i.e. 900–950 W/m^2), the performance of PI is as similar to that of SMC. Further, none of the controllers produce in any over/undershoots. Hence, both PI and SMC reveal very good performance. However, for a wide

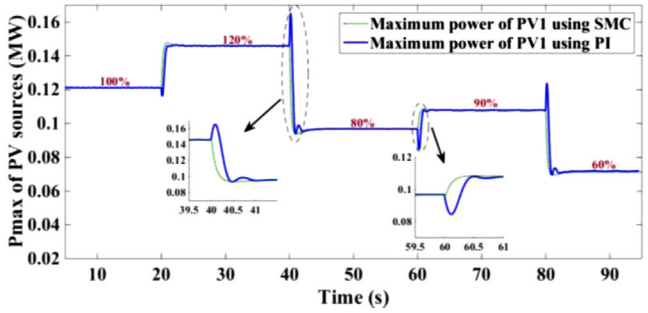

FIGURE 14 Maximum PV power control using PI and SMC for wide variations of irradiance levels

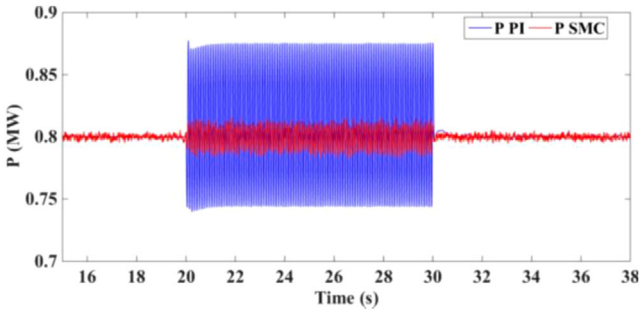

FIGURE 15 Grid power under step change in frequency using PI controller and SMC

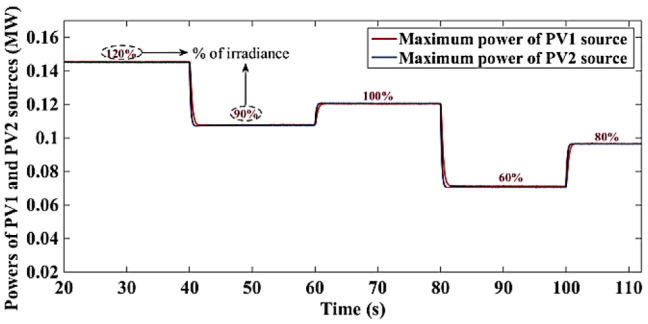

FIGURE 16 Maximum powers of PV_1 and PV_2 at different insolation

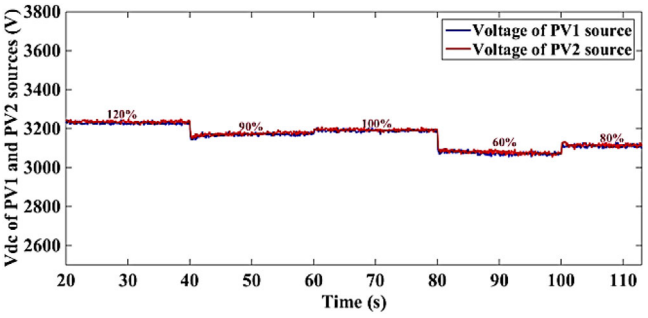

FIGURE 17 Voltages of corresponding maximum powers of PV_1 and PV_2 at different irradiance levels

variation of irradiance levels (say, 120% to 80%), the same PI controller delivers power with high over/undershoots as shown in Figure 14. This is because, PI is a fixed gain controller and its parameters are tuned only for specific irradiance condition. This type of performance of PI control may trigger the over current protection circuit in the system. Therefore it ends up disconnecting the converter from the system entirely; otherwise, the switching devices in MLI will get damaged, which leads to discontinuity in operation. On the contrary, PV power extraction using SMC gives a smooth and fast response as shown in Figure 14. This is due the capability of SMC controller to adapt its gains according to the distance of the error from the defined error sliding surface. Therefore, for a wide variation in different irradiance levels, the SMC exhibits superior performance without over/undershoots in PV power response.

7.1.2 | Robustness of SMC

The robustness of SMC is confirmed by observing the insensitivity of SMC towards the system uncertainties and it is verified by considering a case of small change in grid frequency in proposed grid connected SSPS MLI system. In order to confirm robustness of SMC, its performance is compared with conventional PI controller for controlling the grid connected MLI. Whenever grid frequency is allowed to a continuous variation from 50 to 50.25 Hz, PI controller offers stringent oscillations in response of grid power as shown in Figure 15. Whereas the control of grid connected MLI using SMC, the oscillations in the power response are very few. Since SMC is a variable gain controller, it can adjust its gains according to system parameter variations and offers robustness irrespective of the system uncertainties. It is confirmed by observing Figure 15, which shows the power response under the control of SMC and PI during frequency oscillations during 20 to 30s.

7.1.3 | Individual PV powers and corresponding voltages of PV sources of SSPS MLI

The maximum powers deliver from PV_1 and PV_2 sources of SSPS MLI at various irradiance levels are shown in Figure 16. Whenever the irradiance is decreased from 120% to 90% at 40 s, the PV_1 and PV_2 sources respond quickly to deliver the maximum power from 145.68 to 107.22 kW under efficient SMC controller. Beyond 40 s, the solar insolation is considered as constant till 60 s, hence the PV power output is constant (107.22 kW) as depicted in Figure 16. For increase of insolation from 90% to 100% at 60 s, the PV power increases from 107.22 to 119.97 kW within a few cycles. Hence, under the effective control of established SMC, both PV_1 and PV_2 sources delivered the maximum powers corresponding to increase or decrease of irradiance. Further, from Figure 16 it can be observed that SSPS MLI facilitates uniform delivery of maximum power from both PV_1 and PV_2 sources. Hence it confirms the equal utilisation of PV_1 and PV_2 sources in SSPS MLI. The proposed system maintains the stability at each irradiance level and generates desired PV powers without steady state error. Further, in order to examine the satisfactory performance of the established SMC control strategy under variation in insolation levels, the output voltages of PV_1 and PV_2 sources are presented in Figure 17. During irradiance levels of 120%, 90%, 100%, 60%, and 80%, the output voltages of PV_1 and PV_2 sources are 3234, 3180, 3200, 3085, and 3134 V respectively as shown in Figure 17. Theses output voltages are correspond to maximum powers delivered from PV_1 and PV_2 sources, so that the photovoltaic sources respond correctly according to their PV characteristics curves as shown in Figure 10. Hence, with the proposed SMC strategy, both PV_1 and PV_2 sources generate maximum PV powers and their corresponding PV voltages for wide variations of irradiance levels. This is because, SMC can

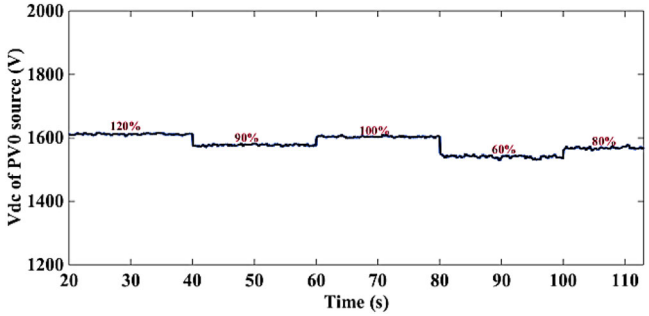

FIGURE 18 Voltage of corresponding maximum power of PV_0 at different irradiance levels

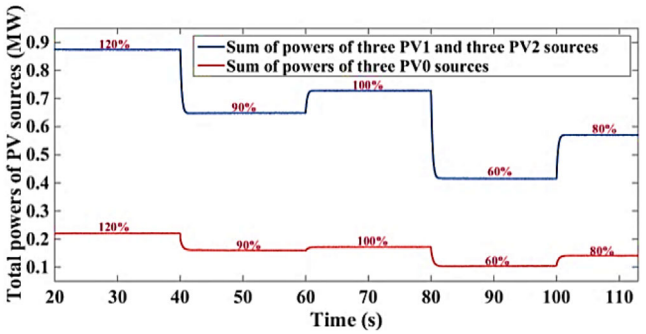

FIGURE 19 Sum of maximum powers of PV sources of three-phase asymmetric SSPS MLI

adapt its gains according to the error (V_{pv}–V_{pvref}) and change in irradiance levels and exhibit extraordinary performance while providing outputs with very low over/undershoots and settle within a few cycles. Similarly, the voltage at the corresponding maximum power of PV_0 source at various insolation levels can be observed in Figure 18.

7.1.4 | Total maximum powers of PV sources

Figure 19 shows the sum of the powers extracted from three PV_1, three PV_2 sources and three PV_0 sources of three-phase asymmetric SSPS MLI using common SMC scheme. The total power of three PV_1 and three PV_2 sources at insolation levels of 120%, 90%, 100%, 60%, and 80% is 874.08, 643.32, 719.82, 417.42, and 567.36 kW respectively, as shown in Figure 19. The total power of three PV_1 and three PV_2 sources at various irradiance levels is equal to six times the individual maximum power of PV_1 (or PV_2). This ensures that the established common SMC control scheme accurately tracks the desired maximum powers from all six equal rated PV sources (i.e. three PV_1 and three PV_2) at various irradiance levels. Further, whenever the insolation is decreased from 120% to 90% at 40 s, the net power of all six PV_1 sources is decreased quickly from 874.08 to 643.32 kW and this total power is maintained constant till 60 s since irradiance level (90%) is maintained constant as depicted in Figure 19. At 60 s, because of increase in irradiance level from 90% to 100%, the total PV power also rapidly increases from

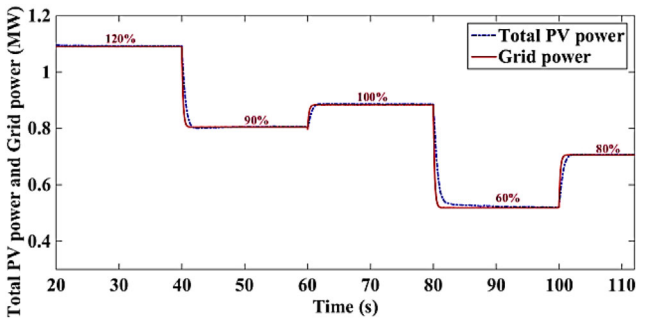

FIGURE 20 Generated total PV power (P_{ref}) and grid power (P_g) at various irradiance levels

643.32 to 719.82 kW. The quick change in the total PV power because of irradiance changes is confirmed that the simultaneous and quick common control action of the SMC acts on all equal rated PV sources. A similar observation is recorded for the total PV power extracted from three PV_0 sources of three-phase SSPS MLI under the control of another SMC is shown in Figure 19. Therefore, the feasibility in common control of maximum PV powers of all the same rated PV sources using the established SMC scheme is verified successfully.

7.1.5 | Grid power

Figure 20 represents the PV power (P_{ref}) supplied to grid and grid power (P_g). Supplied PV power is the sum of maximum powers of all the asymmetric PV sources connected to the three-phase SSPS MLI. From Figure 20, it can be observed that, whenever the irradiance is considered as constant at 120%, the total PV power generated from all PV sources is 1.0926 MW and it is successfully injected to grid by effective control of SSPS MLI using SMC. At 40 s, as irradiance is decreased from 120% to 90%, the total PV power (P_{ref}) also decreases from 1.0926 to 0.8041 MW and the grid power follows exactly the same pattern of P_{ref}. Similarly, when irradiance increases from 90% to 100% at 60 s, the grid power increases from 0.8041 to 0.8917 MW as P_{ref} is increased to the same value. Hence, as the irradiance changes, P_{ref} also changes and three-phase SSPS MLI is controlled by SMC in such a way that the grid power also changes according to the new P_{ref}. From Figure 20 it can be concluded that for wide variations in irradiance levels, the total PV power generated is completely supplied to grid and grid power (P_g) reaching a new steady-state within a few cycles, without over/undershoots. Therefore, the objective of the proposed closed-loop control system using SMC is achieved in MATLAB/Simulink environment.

7.2 | Real-time validation

The proposed SSPS MLI based grid interfaced PV system under the control of SMC scheme is verified in real-time environment using hardware-in-loop (HIL) setup with two OP4500

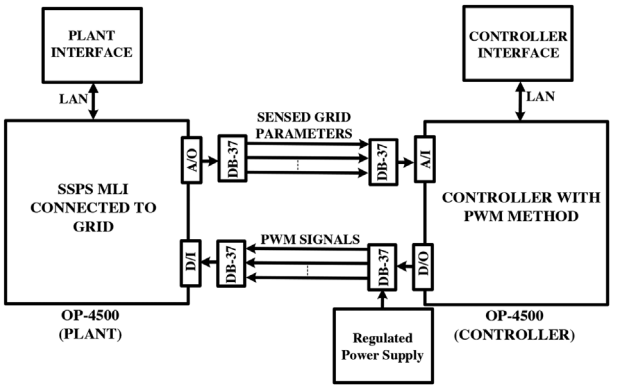

FIGURE 21 Schematic diagram of implementation of proposed system on OPAL-RT platform

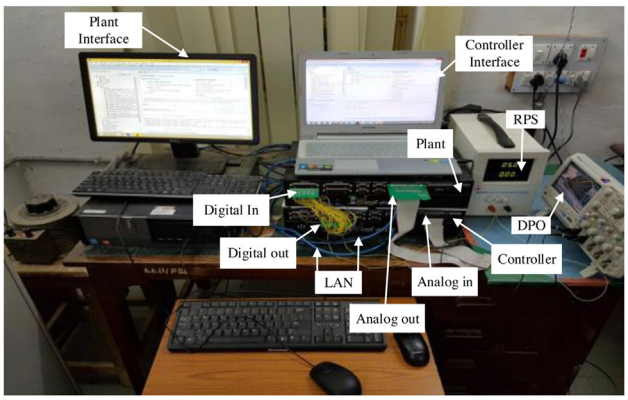

FIGURE 22 Photograph of implementation of proposed system on OPAL-RT platform

modules. The schematic diagram and its photograph are shown in Figures 21 and 22 respectively. In HIL structure, one of the OPAL-RT modules performs as a plant which includes SSPS MLI based grid tied PV system. The other module works as controller for maximum PV power extraction and generates PWM switching signals for MLI. The sensed signals generated from plant system are given to controller system which generates necessary control actions. The communication between controller and plant systems (i.e. two OP4500 modules) is processed through DB-37 connector and this whole setup is known as hardware-in-loop (HIL) arrangement. The successful execution of the MLI based grid connected closed-loop control system in HIL is done by considering the sampling-time as 50 μs. The system parameters considered in HIL platform are the same as the parameters considered in MATLAB/simulation case study. HIL results are recorded using digital storage oscilloscope (DSO).The PWM strategy is designed in such a way that the three-phase SSPS MLI generates 11-level output phase-voltages as shown in Figure 23.

Figure 24 shows the variation of maximum PV power of PV_1 under the control of SMC and PI during decreasing irradiance conditions. From Figure 24(a,c) it is evident that whenever the irradiance is decreasing, PI controller delivers a large overshoot in PV power with a very large settling time which is not acceptable in real case. This kind of high overshoots can damage the switching devices of MLI, leading to discontinuous operation of the system. In order to avoid this, an additional protection system is required, which leads to a rise in total cost and system complexity. On the other hand, the control of PV power using SMC scheme results in very good response without any overshoot and settles the new desired PV power within a few cycles as shown in Figure 24(b,d). In the same way, PI controller delivers a large undershoot in PV power response as represented in Figure 25(a,c) during insolation which increases from 100% to 120% and 60% to 100% respectively. Whereas the control of PV power using SMC, results in improved response without undershoot and with faster dynamic response compared to PI controller and it is confirmed by observing Figure 25(b,d).

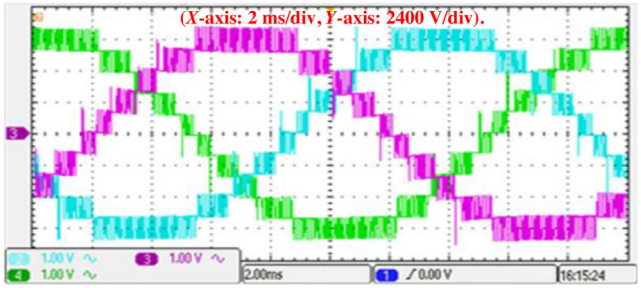

FIGURE 23 Three-phase voltages of eleven-level SSPS ML

The performance of MLI based grid connected system under the control of SMC scheme and PI controller during grid frequency variations is presented in Figure 26. While grid frequency is varying continuously, which characterizes modal frequency fluctuations, PI controller causes quite oscillatory performance with very large oscillations in grid power response as shown in Figure 26(a). These huge power fluctuations may activate the protection circuit of MLI. Therefore, the response of the conventional PI control, which cannot adapt its gains, is a potential candidate to generate uncertainty in the system by disconnecting the MLI, which delivers power to the grid. On the other hand, the system with SMC provides nearly a smooth power with very few deviations as shown in Figure 26(b), thus confirming that the inverter remains connected to grid during the grid frequency variations. Therefore, it can be confirmed that SSPS-RSC MLI based grid interfaced PV system under SMC can operate more stably and can overcome the instabilities.

Figure 27 represents the variation of individual maximum powers of PV_1, PV_2 and PV_0 sources at various irradiance levels. From Figure 27 it is observed that the individual powers delivered from PV_0, PV_1 and PV_2 at the considered irradiance level of 1000 W/m^2 are 57.3, 119.97, and 119.97 kW respectively. Hence, the asymmetric sources deliver powers in the ratio of their voltage levels that is, 1:2:2. Similarly, at other irradiance levels also the PV sources generate the power according to voltage ratio (i.e. 1:2:2) which can be observed in Figure 27. Therefore, asymmetric SSPS MLI offers uniform burden on the PV sources at the considered insolation levels in real-time environment. Further, Figure 28 shows the voltages which are corresponding to the maximum power of PV sources at

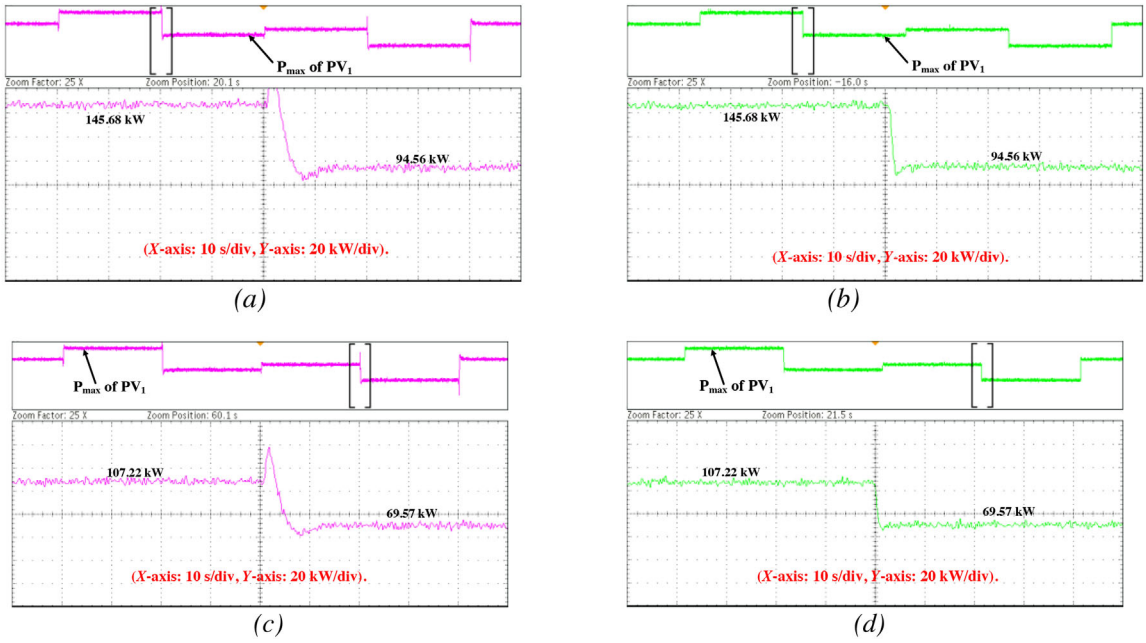

FIGURE 24 Performance of PI and SMC for control of maximum power of PV_1 source during irradiance decreasing conditions. (a) Irradiance changes from 120% to 80% with PI. (b) Irradiance changes from 120% to 80% with SMC. (c) Irradiance changes from 90% to 60% with PI. (d) Irradiance changes from 90% to 60% with SMC

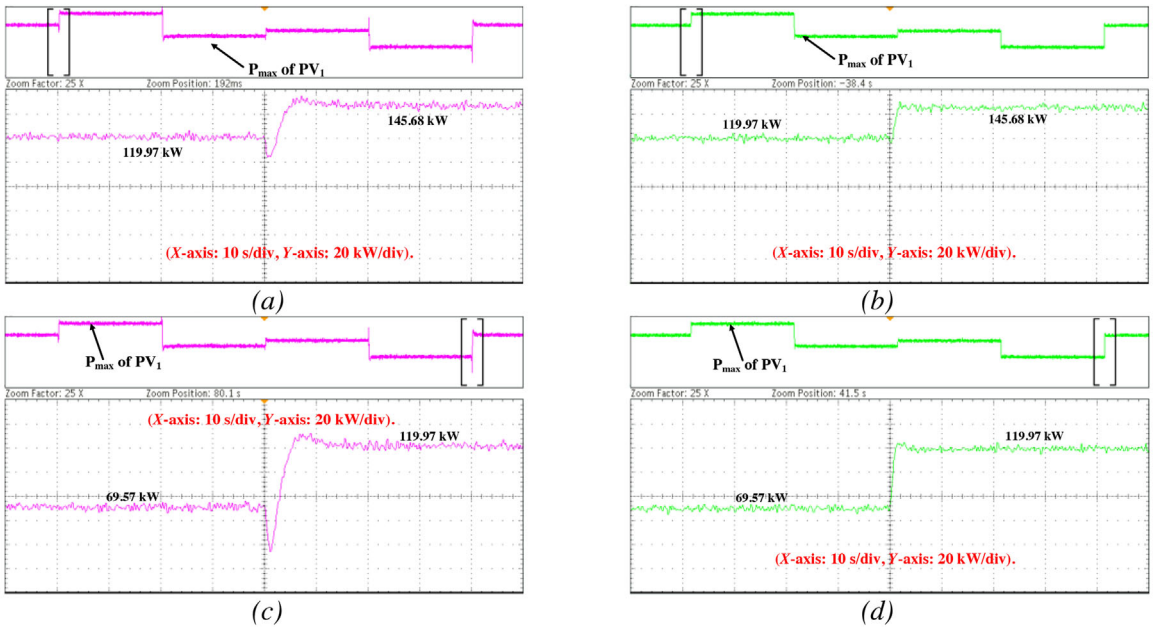

FIGURE 25 Performance of PI and SMC for control of maximum power of PV_1 source during irradiance increasing conditions. (a) Irradiance changes from 100% to 120% with PI. (b) Irradiance changes from 100% to 120% with SMC. (c) Irradiance changes from 60% to 100% with PI. (d) Irradiance changes from 60% to 100% with SMC

various insolation levels. These voltages are also in the ratio of 1:2:2 and contribute to generate an eleven-level output voltage shown in Figure 23. Therefore, from Figures 27 and 28, it is confirmed that even though there is a wide variation of insolation levels in HIL based real-time environment, the steady-state values of individual PV powers and the corresponding voltages are according to the PV characteristics shown in Figure 10. This is because; the contribution of SMC is appreciable in realizing the maximum powers without steady-state error.

Figure 29 represents the total power of three PV_0 sources, total power of three PV_1 and three PV_2 sources of three-phase SSPS MLI and grid power (P_g). From Figure 29 it can be

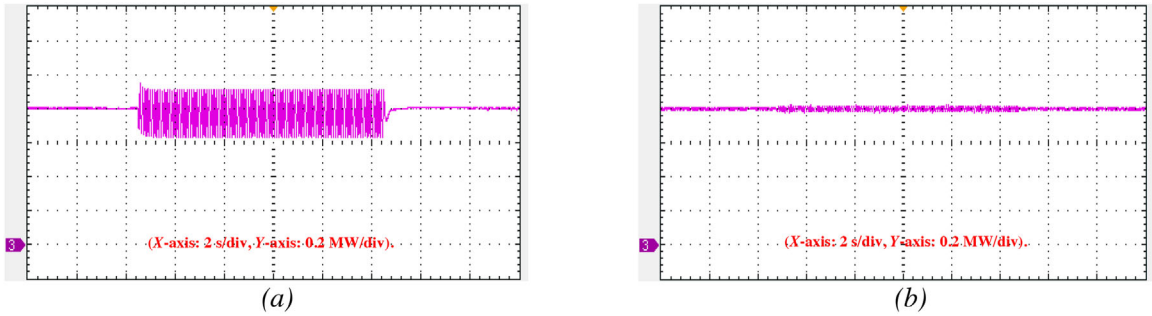

FIGURE 26 Power feeding by SSPS MLI to the grid during frequency oscillations with (a) PI and (b) SMC (a) Oscillations in grid power under PI control (b) Oscillations in grid power under SMC

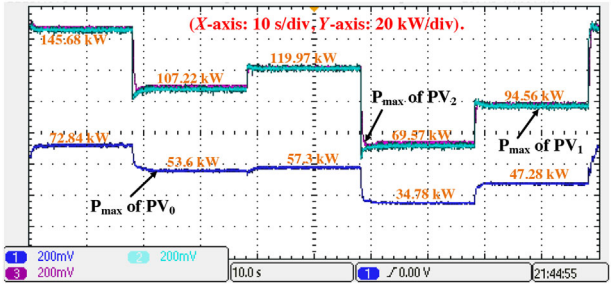

FIGURE 27 Maximum powers of PV_1, PV_2 and PV_0 at different irradiance levels

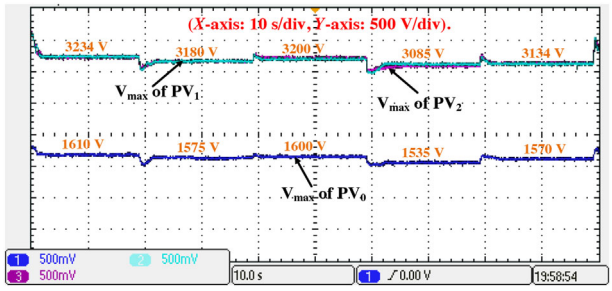

FIGURE 28 MPPT voltages of PV_1, PV_2 and PV_0 of SSPS MLI

observed that, at the irradiance levels of 120%, 90%, 100%, 60%, and 80%, the total power of three PV_1 and three PV_2 sources are 0.874, 0.6433, 0.7198, 0.4174, and 0.5674 MW respectively. And these powers are exactly equal to six times the maximum power of a single PV_1 (or PV_2) source at various irradiance levels. Hence, it is confirmed that all three PV_1 and three PV_2 sources of the three-phase SSPS MLI operate at the desired maximum power operating point using a common SMC. Similarly, from Figure 29 it can be confirmed that the total power of three PV_0 sources of the three-phase SSPS MLI is equal to three times the maximum power of single PV_0 source under various irradiance conditions. Hence, all the PV_0 sources also operate at the desired maximum power point using another common SMC strategy. Hence, the common sliding mode control philosophy is effective in controlling the maximum PV powers which are

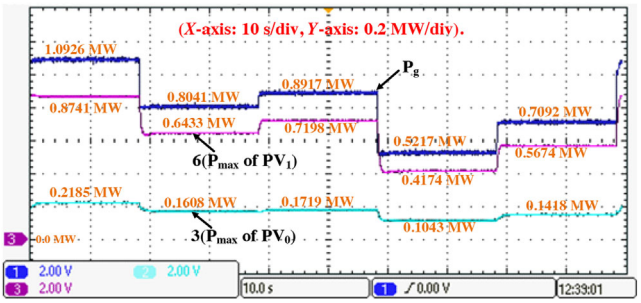

FIGURE 29 Grid power (P_g), sum of maximum powers of three PV_1 and three PV_2 sources and sum of maximum powers of three PV_0 sources of three-phase SSPS MLI

extracted from all equal rated PV sources for a wide range of irradiance levels.

Hence, the established SMC scheme ensures maximum possible utilisation of PV sources in HIL environment. Further, from Figure 29 it is observed that, for a considered irradiance of 120%, the total generated maximum power (i.e. 0.8741 MW + 0.2185 MW) from all PV sources (i.e. $3PV_1$, $3PV_2$, and $3PV_0$) is equal to grid power (1.0926 MW). Similarly, for other irradiance conditions, the total generated maximum PV power is equal to grid power (P_g). Since the established SMC schemes used the feedback linearization technique for deriving I_{dcref} and for control of SSPS MLI, the PV generator quickly and accurately tracks the new power and it is successfully injected into the grid. Therefore, from Figures 24–29, it can be concluded that the closed-loop control of proposed SSPS MLI based grid interfaced PV system under designed SMC strategy is satisfactory for a wide variations of irradiance levels in real-time hardware-in-loop platform. Similar observation is found in off-line simulation results presented in Section 7.1.

8 | CONCLUSION

In this paper, a comparative analysis was made to select superior RSC-MLI topology for grid connected PV application. The chosen SSPS RSC-MLI can be an alternative to conventional CHB MLI in the application of medium voltage and high PV

power feeding to grid. This paper confirms the feasibility in the establishment of non-linear common sliding mode control scheme for regulation of single-stage PV source during irradiance changes. This is because of the linearization of the non-linear PV system using feed-back linearization scheme. MATLAB/Simulink and real-time results prove that under wide variations of irradiance conditions, the performance of SMC is superior to that of PI controller which delivers higher under/over shoots in the power response. The desired maximum power tracking from all asymmetric PV sources is possible under efficient control of common SMC strategy. Further, the simulation and real-time results thus obtained ensure that total PV power generated from all input PVs of the three-phase SSPS topology is successfully injected into grid with ease.

REFERENCES

1. Vijeh, M., et al.: A general review of multilevel inverters based on main submodules: Structural point of view. IEEE Trans. Power Electron. 34(10), 9479–9502 (2019)
2. Kumar Gupta, K., et al.: Multilevel inverter topologies with reduced device count: A review. IEEE Trans. Power Electron. 31(1), 135–151 (2016)
3. Sathik, J., et al.: An assessment of recent multilevel inverter topologies with reduced power electronics components for renewable applications. Renewable Sustainable Energy Rev. 82, 3379–3399 (2018)
4. Khodaparast, A., et al.: A step-up switched-capacitor multilevel inverter based on 5-level T-type modules. IET Power Electron. 12(3), 483–491 (2019)
5. Choi, W., Kang, F.: H-bridge based multilevel inverter using PWM switching function. In: *Proceedings of the 31st International Telecommunications Energy Conference*. Incheon, South Korea. pp. 1–5 (2009)
6. Babaei, E.: A cascade multilevel converter topology with reduced number of switches. IEEE Trans. Power Electron. 23(6), 2657–2664 (2008)
7. Sing, L. S: Single-stage switched-capacitor module (S^3CM) topology for cascaded multilevel inverter. IEEE Trans. power Electron. 33(10), 8204–8207 (2018)
8. Sandeep, N., Yaragatti, U.R.: Design and implementation of active neutral point-clamped nine-level reduced device count inverter: An application to grid integrated renewable energy sources. IET Power Electron. 11(1), 82–91 (2018)
9. Phanikumar, C., et al.: A Hybrid 9-level, 1-ϕ Grid connected multi-level inverter with low switch count and innovative voltage regulation techniques across auxiliary capacitor. IEEE Trans. Power Electron. 34(3), 2159–2170 (2019)
10. Hota, A., et al.: An improved three-phase five-level inverter topology with reduced number of switching power devices. IEEE Trans. Ind. Electron. 65(4), 3296–3305 (2018)
11. Najafi, E., Yatim, A. H. M.: Design and implementation of a new multilevel inverter topology. IEEE Trans. Ind. Electron. 59(11), 4148–4154 (2012)
12. Lee, S. S., et al.: Hybrid cascaded multilevel Inverter (HCMLI) With Improved Symmetrical 4-Level Submodule. IEEE Trans. Power Electron. 33(2), 932–935 (2018)
13. Gui-Jia, S., Multilevel DC-link inverter. IEEE Trans. Ind. Appl. 41(3), 848–854 (2005)
14. Gui-Jia, S., Multilevel DC link inverter. In: *Proc. IEEE IAS Annu. Meet.Conf. Record Ind. Appl. Conf.* 2, 806–812 (2004)
15. Hinago, Y., Koizumi, H.: A single-phase multilevel inverter using switched series/parallel dc voltage sources. IEEE Trans. Ind. Electron. 57(8), 2643–2650 (2010)
16. Xiao, B., et al.: Modular cascaded H-Bridge multilevel PV inverter with distributed MPPT for grid-connected applications. IEEE Trans. Ind. Application. 51(2), 1722–1731 (2015)
17. Villanueva, E., et al.: Control of a single-phase Cascaded H-Bridge multilevel inverter for grid-connected photovoltaic systems. IEEE Trans. Ind. Electron. 56(11), 4399–4406 (2009)
18. Shi, Y., et al.: High-frequency-link-based grid-tied PV system with small DC-Link capacitor and low-frequency ripple-free maximum power point tracking. IEEE Trans. Power Electron. 31(1), 328–339 (2016)
19. Liu, L., et al.: Decoupled active and reactive power control for large-scale grid-connected photovoltaic systems using cascaded modular multilevel converters. IEEE Trans. Power Electron. 30(1), 176–187 (2015)
20. Coppola, M., et al.: An FPGA-Based advanced control strategy of a grid-tied PV CHB Inverter. IEEE Trans. Power Electron. 31(1), 806–816 (2016)
21. Iman-Eini, H., Tennakoo, S. B.: Investigation of a cascaded H-bridge photovoltaic inverter under nonuniform insolation conditions by hardware-in-the-loop test. Int J Electric Power Energy Syst. 105, 330–340 (2019)
22. Alonso, O., et al.: Cascaded H-Bridge multilevel converter for grid connected photovoltaic generators with independent maximum power point tracking of each Solar Array. In: Proceedings of IEEE 34th Annual Power Electronics Specialists Conference. Mexico. pp. 731–735 (2003)
23. Moharana, A., Das, P.K.: Input-Output Linearization and Robust Sliding-Mode Controller for the VSC-HVDC Transmission Link. IEEE Trans. Power. Deliv. 25(3), 1952–1961 (2010)
24. Mishra, S., Sekhar, P.C.: Sliding mode based feedback linearizing controller for a PV System to Improve the Performance under Grid Frequency Variation. In: *IEEE International Conference on Energy, Automation, and Signal (ICEAS)*. Bhubaneswar. (2011)
25. Hannan, M.A., et al.: Fuzzy logic inverter controller in photovoltaic applications: Issues and recommendations. IEEE Access. 7, 24934–24955 (2019)
26. Veerachary, M., et al.: Neural-network-based maximum-power-point tracking of coupled-inductor interleaved-boost converter-supplied PV system using fuzzy controller. IEEE Trans. Ind. Electron. 50(4), 749–758 (2003)
27. Sun, Y., et al.: Artificial neural network for control and grid integration of residential solar photovoltaic systems. IEEE Trans. Sustainable Energy. 8(4), 1484–1495 (2017)
28. Benaissa Mohammed, O., et al.: A comparative investigation of maximum power point tracking techniques for grid connected PV system under various weather conditions. In: *IEEE Int. Conf. Electrical Engineering – (ICEE-B)*. Boumerdes (2017)
29. Be´langer, J., et al.: "The what, where and why of real-time simulation" Available at https://blob.opalrt.com/medias/L00161_0436.pdf

How to cite this article: Gowd, G. E., Sreenivasarao, D., Vemuganti, H. P.: Sliding mode controller for extraction and supply of photovoltaic power using switched series parallel sources reduced switch count multilevel inverter. *IET Power Electron.* 2021;14:834–850. https://doi.org/10.1049/pel2.12068